

## Radiation Pressure Acceleration in the Light-Sail Regime.

M. Zepf,<sup>1</sup> M. Borghesi<sup>1</sup>, P. McKenna<sup>3</sup>, D. Neely<sup>2</sup>, Z. Najmudin<sup>4</sup>, A. P. L. Robinson<sup>2</sup>, R. Prasad<sup>1</sup>, S. Ter-Avetysian<sup>1</sup>, P.F. Foster<sup>1,2</sup>, D.C. Carroll<sup>3</sup>, D. Doria<sup>1</sup>, N. Dover<sup>4</sup>, P. Gallegos<sup>2,3</sup>, J. S. Green<sup>2</sup>, C. A.J. Palmer<sup>4</sup>, L. Romagnani<sup>1</sup>, B. Qiao<sup>1</sup>, K. Quinn<sup>1</sup>, M. Streeter<sup>2,4</sup>, J. Schreiber<sup>4,5</sup>, C. Brenner<sup>2,3</sup>, O. Tresca<sup>3</sup>,

<sup>1</sup>School of Mathematics and Physics, Queen's University Belfast, UK

<sup>2</sup>Central Laser Facility, Rutherford Appleton Laboratory, Oxford, UK

<sup>3</sup>University of Strathclyde, Glasgow, UK

<sup>4</sup>Imperial College of Science, Technology and Medicine, UK

Accelerating objects using radiation pressure exerted by a beam of light has the potential to accelerate objects to velocities approaching the speed of light. While the dream of using this approach to accelerate macroscopic objects such as spacecraft by this means<sup>1</sup> remains far from current technological capabilities, the extreme pressure that can be exerted by the most powerful femtosecond lasers ( $P=I/c > 100\text{Gbar}$ ) has made this feasible for micrometer diameter and nanometer thickness foils<sup>2</sup>. We present the first experimental evidence of foil acceleration in the light-sail regime where the whole foil exposed to laser radiation is pushed forwards by the pressure exerted by the intense laser pulse. Experimental data displaying the key signatures of the light-sail regime – peaked proton spectra for thin foil interactions.

Big strides have been made since the first observation of laser accelerated proton and ion beams<sup>3</sup>, which have been shown to have exceptionally good emittance<sup>4</sup> and an ultra-short pulse duration that allows rapidly evolving electric fields to be probed with unprecedented clarity. Until recently the dominant mechanism in most proton acceleration experiments was Target Normal Sheath Acceleration (TNSA), which relies on the laser energy first, being converted into a beam of relativistic electrons on a target foil. When these electrons exit the rear of the foil, a sheath field in excess of  $10^{12}\text{V/m}$  is formed. Species with the highest charge/mass ratio (typically protons due to impurities) are preferentially accelerated to energies, which have been shown to reach 60 MeV for 500J/500fs petawatt-class lasers. The TNSA mechanism has the advantage of being robust and producing beams of excellent transverse emittance, but only scales to higher energies relatively slowly<sup>6</sup> ( $E \propto I^{1/2}$ ). Furthermore, while the beams have good longitudinal emittance, this is obtained by a

combination of extremely short pulse duration (<1ps) and large energy spread. In particular, while the overall efficiency can reach values approaching 10%, the efficiency into the spectral region near the maximum energy is many orders of magnitude lower.

A completely separate mechanism of accelerating ions co-exists during high-intensity laser interactions – Radiation Pressure Acceleration. Radiation pressure effects have previously been recognised as being important for the dynamics of the interaction of the laser with a solid target and leads to a rapid deformation (denting) of the plasma surface. In the thick target regime (‘holeboring’) one obtains a robust non-relativistic estimate of the holeboring velocity.

$$v = \left( \frac{2I}{\rho c} \right)^{1/2},$$

based on the momentum balance ( $p_{\text{beam}} = p_{\text{Laser}}$ ) between the accelerated ions and the laser momentum. Note that the holeboring velocity depends solely on root of the laser intensity (I) and target density ( $\rho$ ).

In the limit of thin foils the laser accelerates all the ions in the laser path and the acceleration now scales as if the foil were being pushed as a whole (the so-called ‘light-sail’ regime). Consequently, momentum balance considerations show that the change in momentum of the entire foil must now balance the laser momentum resulting in

$$\frac{dp}{dt} = \frac{2I}{\sigma}$$

as a non-relativistic estimate for the light-sail regime. Clearly, acceleration becomes more effective in both cases with reduced areal mass density  $\sigma$  (or density  $\rho$  for holeboring) as long as the target remains opaque to the laser.

In contrast to the  $I^{1/2}$  for the TNSA mechanism, the ion energy in the light-sail regime thus scales quadratically with laser intensity (or somewhat more slowly once relativistic effects have been taken into account). This far more rapid scaling suggests that for higher intensities RPA should become the dominant effect on ion dynamics in laser interactions with thin solid foils, and numerical simulations have predicted that for the interaction of a linearly polarised pulse ( $I \sim 10^{23} \text{Wcm}^{-2}$ ) with a thin foil relativistic ions with GeV/u will be produced (u: atomic unit of mass)

However, at lower intensities and for linear polarisation the efficient production of relativistic electron bunches due to  $v \times B$  force results in TNSA co-existing with RPA. TNSA decompresses the foil during the pulse, resulting in early transparency and termination of the

RPA process and a masking of the experimental signature of RPA due to TNSA accelerated particles.

This limitation can be overcome in principle by using circular polarisation at normal incidence. In circular polarisation the magnitude of E and B are constant during an optical cycle and hence the ponderomotive force no longer oscillates twice per optical cycle. In effect the laser interaction with the target electrons becomes a quasi-static push, resulting in the offset of the target electrons with respect to their parent ions. Consequently, TNSA is suppressed and it should be possible to create peaked, quasi-monoenergetic ion and proton spectra at lower intensities. From analytical scalings and numerical simulations using 1D PIC codes, the RPA signature of peaked, mono-energetic features should be clearly distinct and observable at intensities around  $10^{19} \text{ Wcm}^{-2}$ .

In practice observation of radiation pressure acceleration is complicated by the fact that typical high-power lasers have either Gaussian or, more typically, Airy-type radial profile in the laser focus. The intensity non-uniformity of such a focus leads to non-uniform laser pressure on the thin foil and consequently to deformation of the thin foil. This leads to a small oscillating electric field component reappearing in the electron motion and consequently the production of relativistic electrons, which drive an (albeit weaker) TNSA expansion of the foil. Consequently the experimental observation of a clear transition from the TNSA to the RPA regime requires intensities the transition into the light-sail regime with intensities  $I \gg 10^{20} \text{ Wcm}^{-2}$ .

Our experiments were performed on the ASTRA-GEMINI facility, which produces pulses with energies up to 15J and pulse duration close to 30 fs. The laser was focused using an F/2 parabola on thin foil targets (typically C with 10-50nm thickness) and the accelerated ions and protons were detected using a Thomson parabola placed on the laser axis. The contrast was enhanced using a plasma mirror system consisting of two anti-reflection coated pieces of glass with s-polarised light incident. This system enhanced the contrast by a factor of  $10^4$  and had a throughput of 50-60%. The peak intensities on target was  $> 2 \cdot 10^{20} \text{ Wcm}^{-2}$  with an peak to ASE contrast of  $10^{12}:1$ . The laser was circularly polarised to achieve a quasistatic radiation pressure. In this regime one would expect to observe clear light-sail acceleration for carbon foils of 10s of nm thickness. Figure 1 shows proton spectra taken at peak intensity, displaying a clear monoenergetic peak at 9MeV and 4 MeV respectively and extending up to maximum energies of 20 MeV. These energies are in good agreement with numerical simulations of the interaction and show for the first time that a relatively narrow peak can be generated by the RPA mechanism.

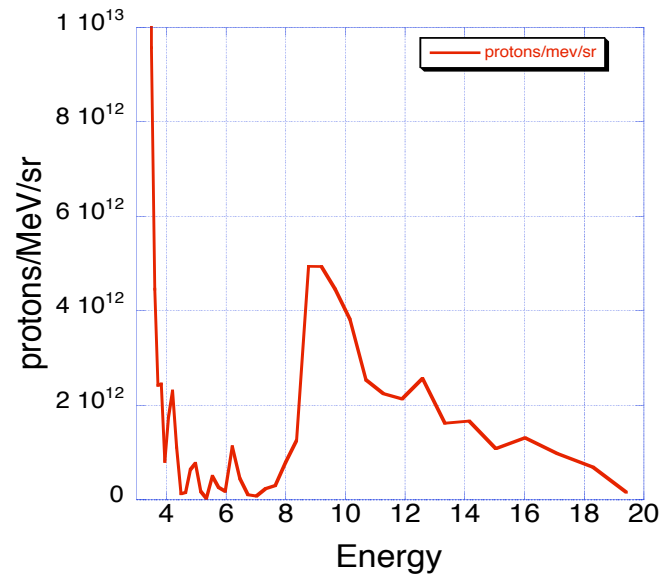


Figure 1: Proton spectrum observed in the light-sail regime. A clear proton peak is observed in agreement with PIC simulations. The gap to lower energies is consistent with the radiation pressure accelerating the whole foil in the centre of the focus. PIC simulations of the interaction show that the low energy component below 4 MeV is due to a low level TNSA component taking place several FWHM away from the laser spot.

The absence of a proton signal between 4 and 8 MeV is consistent with whole foil acceleration in the centre of the spot. PIC simulations suggest that the spectrum on the laser axis is indeed almost completely free of a low energy component in contrast to TNSA interactions. The proton signal below 4 MeV in our experimental data is attributed to the signal produced far from the laser spot by the residual hot electrons. The deformation of the foil during the interaction leads to the wings of the focal spot interacting at oblique incidence. Hence the suppression of hot electron production is imperfect and the hot electrons propagate through the target and drive a weak TNSA expansion. PIC simulations show that at large radii the protons accelerated by this weak TNSA field propagate along the target normal and are hence detected by the Thomson Parabola.

In conclusion, we have observed the first peaked proton spectra in the RPA regime providing a significant step forward in the field laser proton and ion acceleration. Building on these results, the rapid scaling of RPA is expected to lead to beams with energies exceeding 100MeV in the near future.

- 1) G.Marx.. *Nature*, 211:22, (1966).
- 2) APL Robinson et al, *New J. Phys.* **10** 013021 (2008)
- 3) Snavely R.A. *et al*, *Phys. Rev. Lett.* **85**, 2945 (2000)
- 4) Cowan T. et al., *Phys. Rev. Lett* **92**, 204801 (2004)
- 5) Robson L. *et al.*, *Nature Physics* **3**, 58-62, (2007)